87024

ANL/ET/PP--87024

Dynamic Stability of Electrodynamic Maglev Systems*

by

Y. Cai, S. S. Chen, T. M. Mulcahy, and D. M. Rote
Argonne National Laboratory
9700 South Cass Avenue, Argonne, Illinois 60439

Submitted to ASME Trans., Journal of Applied Mechanics.

*Work performed under the sponsorship of the U.S. Army Corps of Engineers and the Federal Railroad Administration, through interagency agreements with the U.S. Department of Energy.

DISCLAIMER

DYNAMIC STABILITY OF ELECTRODYNAMIC MAGLEV SYSTEMS

Y. Cai, S. S. Chen, T. M. Mulcahy, and D. M. Rote
Argonne National Laboratory
Argonne, IL 60439

ABSTRACT

Because dynamic instabilities are not acceptable in any commercial maglev system, it is important to consider dynamic instability in the development of all maglev systems. This study considers the stability of maglev systems based on mathematical models and experimental data. Divergence and flutter are obtained for coupled vibration of a three-degree-of-freedom maglev vehicle on a guideway consisting of double L-shaped aluminum segments. The theory and analysis for motion-dependent magnetic-force-induced instability developed in this study provides basic stability characteristics and identifies future research needs for maglev systems.

INTRODUCTION

For safety, maglev systems should be stable. The repulsive levitation system, or the so-called electrodynamic system (EDS), is often thought to be inherently stable. However, its response to perturbations is frequently unstable and susceptible to catastrophic oscillations, particularly in rectangular-trough configurations (Chen et al., 1992; Cai et al., 1995). So far, only a few analytical and experimental studies have been performed to gain an understanding of the stability characteristics of EDS-type maglev systems (Davis and Wilkie, 1971;

Ohno et al., 1973; Moon, 1974 and 1977; Chu and Moon, 1983; Yabuno et al., 1989; Cai and Chen, 1993 and 1995).

Motion-dependent magnetic forces are the controlling elements in the stability of maglev systems in which vehicles travel at high speed. At this time, very limited studies have been published and many stability issues remain unresolved. Therefore, the theory of motion-dependent magnetic-force-induced instability which consists of both quasistatic motion and unsteady motion theories (Chen, 1987) is developed for application to maglev systems in this paper. This integrated analytical/experimental study presents a systematic method on the stability of maglev systems and answers a series of questions on maglev stability.

Simplified vehicle models were considered in order to gain an understanding of stability characteristics for maglev systems. Divergence and flutter are obtained from analytical solutions for coupled vibration of a three-degree-of-freedom maglev vehicle on a guideway consisting of double L-shaped aluminum segments, and compared with results of both numerical simulation and experimental data.

MOTION-DEPENDENT MAGNETIC FORCES

Motion-Dependent Magnetic-Force Coefficients

Magnetic forces are needed for any vehicle dynamics analysis, guideway structural design, design of fastenings, and prediction of ride quality. These force components are considered from the standpoint of vehicle stability.

As an example, consider a rigid body vehicle with six degrees of freedom, three translations, u_x, u_y, u_z and three rotation, ω_x, ω_y, ω_z, as shown in Fig. 1. Let U be the vector consisting of the six motion components; i.e.,

$$U = \begin{Bmatrix} u_1 \\ u_2 \\ u_3 \\ u_4 \\ u_5 \\ u_6 \end{Bmatrix} = \begin{Bmatrix} u_x \\ u_y \\ u_z \\ \omega_x \\ \omega_y \\ \omega_z \end{Bmatrix}. \tag{1}$$

The motion-dependent magnetic forces can be written

$$f_i = \sum_{j=1}^{6} \left(m_{ij}\ddot{u}_j + c_{ij}\dot{u}_j + k_{ij}u_j \right). \tag{2}$$

where m_{ij}, c_{ij}, and k_{ij} are magnetic mass, damping, and stiffness coefficients. These coefficients can be obtained analytically, numerically, or experimentally, and are functions of the system parameters (Cai et al., 1992).

Experimental Methods to Measure Motion-Dependent Magnetic-Force Coefficients

Quasistatic Motion Theory. The magnetic forces acting on an oscillating vehicle are equal, at any instant in time, to those of the same vehicle moving with a constant velocity with specific clearances equal to the actual instantaneous values. The magnetic forces depend on the deviation from a reference state of speed and clearance; i.e., the motion-dependent magnetic forces depend only on u_j, but not $\dot{u}_j$ and $\ddot{u}_j$, so that

$$f_i = \sum_{j=1}^{6} k_{ij} u_j. \tag{3}$$

In this case, the magnetic forces are determined uniquely by the vehicle position. All elements of magnetic stiffness k_{ij} can be obtained. To determine k_{ij}, the magnetic force component f_i is measured as a function of u_j. The stiffness, k_{ij}, is given by

$$k_{ij} = \frac{\partial f_i}{\partial u_j}. \tag{4}$$

In general, k_{ij} is a function of U.

Unsteady Motion Theory. The magnetic forces acting on an oscillating vehicle will depend on U, $\dot{U}$, and $\ddot{U}$. The magnetic force based on the unsteady motion theory can be obtained by measuring the magnetic force acting on the vehicle oscillating in the magnetic field. For example, if the displacement component u_j is excited, its displacement is given by

$$u_j = \bar{u}_j \exp\left(\sqrt{-1}\,\omega t\right). \tag{5}$$

The linearized motion-dependent magnetic force of the component f_i acting on the vehicle is given by

$$f_i = \left[a_{ij}\cos\left(\psi_{ij}\right) + \sqrt{-1}\,a_{ij}\sin\left(\psi_{ij}\right)\right]\bar{u}_j \exp\left(\sqrt{-1}\,\omega t\right), \tag{6}$$

where a_{ij} is the magnetic force amplitude and ψ_{ij} is the phase angle between the magnetic force and the vehicle displacement u_j. These values are measured experimentally.

Using Eqs. (2) and (4), we can also write the motion-dependent magnetic force component as

$$f_i = \left(-m_{ij}\omega^2 + \sqrt{-1}\,\omega\, c_{ij} + k_{ij}\right)\bar{u}_j \exp\left(\sqrt{-1}\,\omega t\right). \tag{7}$$

Comparing Eqs. (6) and (7) yields

$$c_{ij} = a_{ij}\sin\left(\psi_{ij}\right)/\omega, \qquad m_{ij} = \left[k_{ij} - a_{ij}\cos\left(\psi_{ij}\right)\right]/\omega^2. \tag{8}$$

Based on Eqs. (4) and (8), all motion-dependent magnetic-force matrices can be determined from two experiments: quasistatic motion and unsteady motion.

If m_{ij} and c_{ij} are of no concern, the experiment using quasisteady motion is sufficient to determine k_{ij}.

Quasistatic Motion-Dependent Magnetic-Force Coefficients of Maglev System with L-Shaped Guideway

An experiment, recently conducted at Argonne National Laboratory, investigated the lift, drag, and guidance magnetic forces on an NdFeB permanent magnet moving over an aluminum (6061-T6) L-shaped ring mounted on the top surface of a 1.2-m-diameter rotating wheel (Cai et al., 1992 and 1995).

Based on the magnetic force data obtained from experiments we can calculate the quasistatic motion-dependent magnetic-force coefficients with Eq. (4). The curve fit to both magnetic forces and stiffnesses were derived using polynomial expressions and input into a computer code to simulate coupled vibrations of maglev vehicle (Cai et al., 1992).

STABILITY OF MAGLEV SYSTEMS

Without motion-dependent magnetic forces, the equation of motion for the vehicle consisting of N degrees of freedom can be written

$$[M_v]\{\ddot{U}\}+[C_v]\{\dot{U}\}+[K_v]\{U\}=\{Q\}, \tag{9}$$

where M_V is the vehicle mass matrix, C_V is vehicle damping matrix, K_V is vehicle stiffness matrix, and Q is generalized excitation force.

The motion-dependent magnetic forces are given in Eq. (2). With motion-dependent magnetic forces, Eq. (9) becomes

$$[M_v+M_m]\{\ddot{U}\}+[C_v+C_m]\{\dot{U}\}+[K_v+K_m]\{U\}=\{Q\}, \tag{10}$$

where M_m is the magnetic mass matrix, C_m is magnetic damping matrix, and K_m is magnetic stiffness; their elements are m_{ij}, c_{ij}, and k_{ij}.

Once the magnetic-force coefficients are known, analysis of vehicle stability is straightforward. Equation (10) may be written as

$$[M]\{\ddot{U}\}+[C]\{\dot{U}\}+[K]\{U\}=\{Q\}. \tag{11}$$

In general, M, C, and K are functions of U, $\dot{U}$, and $\ddot{U}$; therefore, a complete solution is difficult to obtain. In many practical situations, in which the threshold parameters associated with dynamic instability are of primary interest, one can ignore all nonlinear terms, such that M, C, and K are independent of vehicle motion.

By premultiplying by $\{\dot{U}\}^T$ and forming the symmetric and antisymmetric components of the matrices

$$[M_1]=\frac{1}{2}\left([M]+[M]^T\right), \qquad [M_2]=\frac{1}{2}\left([M]-[M]^T\right),$$

$$[C_1]=\frac{1}{2}\left([C]+[C]^T\right), \qquad [C_2]=\frac{1}{2}\left([C]-[C]^T\right), \tag{12}$$

$$[K_1]=\frac{1}{2}\left([K]+[K]^T\right), \qquad [K_2]=\frac{1}{2}\left([K]-[K]^T\right),$$

we can separate the terms, giving

$$\{\dot{U}\}^T[M_1]\{\ddot{U}\}+\{\dot{U}\}^T[C_2]\{\dot{U}\}+\{\dot{U}\}^T[K_1]\{U\}$$

$$=-\left(\{\dot{U}\}^T[M_2]\{\ddot{U}\}+\{\dot{U}\}^T[C_1]\{\dot{U}\}+\{\dot{U}\}^T[K_2]\{U\}\right)+\{\dot{U}\}^T\{Q\}. \tag{13}$$

Equation (13) equates rates of work. The terms on the right-hand side of the equation produce a net work resultant when integrated over a closed path through the space {U}, the magnitude depending on the path taken. The forces corresponding to the matrices M_2, C_1, and K_2, appearing on the right-hand side, are thus by definition the nonconservative parts of the forces represented by M, C, and K. The terms on the left-hand side similarly can be shown to give rise to

a zero work-resultant over any closed path, and therefore together are the sum of the rates of work from the potential forces and the rate of change of kinetic energy. Different types of instability can be classified according to the dominant terms in Eq. (13) (Chen, 1987 and Cai et al., 1992).

- Magnetic Damping Controlled Instability (single mode flutter): The dominant terms are associated with the symmetric damping matrix $[C_1]$. Flutter arises because the magnetic damping forces create "negative damping," that is, a magnetic force that acts in phase with vehicle velocity.

- Magnetic Stiffness Controlled Instability (coupled mode flutter): The dominant terms are associated with the antisymmetric stiffness matrix $[K_2]$. It is called coupled mode flutter because at least two modes are required to produce it.

In practical cases, two or more mechanisms may interact with one another, and Eq. (11) is applicable for general cases.

It is noted that maglev systems are subjected to several groups of forces, including magnetic forces, aerodynamic forces, and forces due to guideway perturbation. The theory presented in this paper is applicable to maglev systems when they are subjected to other types of forces. In particular, the aerodynamic effects can be described exactly the same way as those given in Eqs. (1)-(13) and the dynamic response characteristics to aerodynamic forces are similar to magnetic forces (Chen, 1987 and Cai et al., 1992).

SIMPLIFIED VEHICLE MODELS FOR DYNAMIC INSTABILITY

Different vehicles are considered, in order to gain an understanding of stability characteristics. However, only the three-degree-of-freedom vehicle with the double L-shaped sheet guideway is described in this paper.

Figure 2 shows the cross section of a vehicle and guideway. Assume that the vehicle is traveling at a constant velocity along x direction. Two permanent magnets are attached to the bottom of vehicle and provide lift and guidance force F_{L_1}, F_{L_2}, F_{G_1} and F_{G_2} (see Fig. 2). Assuming at the initial state that $h_1 = h_2 = h_0$ and $g_1 = g_2 = g_0$, we can express the geometries of vehicle and guideway as

$$L_1 = L_2 = S = 76.2 \text{ (mm)}, \quad W = 152.4 + S - 2g_0 \text{ (mm)}, \quad H = 0.9\,W \text{ (mm)}$$
$$a = 0.5\,H \text{ (mm)}, \qquad b = 0.5(W-25.4) \text{ (mm)}$$

Equations of motion for this three-degree-of-freedom maglev system can be written as

$$\begin{aligned} m\ddot{z} + C\dot{z} &= F_{L_1} + F_{L_2} - mg \\ I\ddot{\theta} + E\dot{\theta} &= \left(F_{G_1} + F_{G_2}\right)a + \left(F_{L_1} + F_{L_2}\right)b \\ m\ddot{y} + D\dot{y} &= F_{G_1} + F_{G_2} \end{aligned} \tag{14}$$

where m is the mass of the vehicle, C and D are damping ratios; I is the moment of inertia about the center of mass inertia moment of the vehicle [$I = (m/12)(H^2+W^2)$]. F_{L_1}, F_{L_2}, F_{G_1}, and F_{G_2} are lift and guidance forces and are

functions of y and z. At equilibrium position, they are $F_{L10}(y_o,z_o)$, $F_{L20}(y_o,z_o)$, $F_{G10}(y_o,z_o)$, and $F_{G20}(y_o,z_o)$. Applying them to Eqs. (14),

$$F_{L10} = F_{L20}, \qquad F_{L10} + F_{L20} = mg, \qquad F_{G10} = -F_{G20}; \tag{15}$$

therefore,

$$m = \frac{F_{L10} + F_{L20}}{g} = \frac{2F_L(h_o)}{g}. \tag{16}$$

Let

$$z = \frac{1}{2}(u_1 + u_2), \qquad y = u_3, \qquad \theta = (u_1 - u_2)/2b. \tag{17}$$

Equations (14) can be rewritten as

$$\begin{aligned} &m(\ddot{u}_1 + \ddot{u}_2) + c(\dot{u}_1 + \dot{u}_2) = 2\left(F_{L_1} + F_{L_2} - mg\right) \\ &\frac{I}{b}(\ddot{u}_1 - \ddot{u}_2) + \frac{E}{b}(\dot{u}_1 - \dot{u}_2) = 2a\left(F_{G_1} + F_{G_2}\right) + 2b\left(F_{L_1} - F_{L_2}\right) \\ &m\ddot{u}_3 + D\dot{u}_3 = F_{G_1} + F_{G_2}. \end{aligned} \tag{18}$$

Note the reduced dependence of the forces on the new displacements of Eq. (17):

$$F_{L_1} = F_{L_1}(u_1,u_3), \quad F_{L_2} = F_{L_2}(u_2,u_3), \quad F_{G_1} = F_{G_1}(u_1,u_3), \; F_{G_2} = F_{G_2}(u_2,u_3). \tag{19}$$

Let

$$u_i = u_{i0} + v_i \qquad i = 1, 2. \tag{20}$$

The linear approximation of lift and guidance forces can be expressed as

$$\begin{aligned}
F_{L_1} &= F_{L_{10}} + \frac{\partial F_{L_1}}{\partial v_1} v_1 + \frac{\partial F_{L1}}{\partial v_3} v_3 \\
F_{L_2} &= F_{L_{20}} + \frac{\partial F_{L_2}}{\partial v_2} v_2 + \frac{\partial F_{L2}}{\partial v_3} v_3 \\
F_{G_1} &= F_{G_{10}} + \frac{\partial F_{G_1}}{\partial v_1} v_1 + \frac{\partial F_{G1}}{\partial v_3} v_3 \\
F_{G_2} &= F_{G_{20}} + \frac{\partial F_{G_2}}{\partial v_2} v_2 + \frac{\partial F_{G2}}{\partial v_3} v_3.
\end{aligned} \tag{21}$$

Using Eqs. (15) and (21), we can rewrite Eq. (18) as

$$\begin{aligned}
&\ddot{v}_1 + \ddot{v}_2 + \frac{C}{m}\dot{v}_1 + \frac{C}{m}\dot{v}_2 - \frac{2}{m}\frac{\partial F_{L_1}}{\partial v_1} v_1 - \frac{2}{m}\frac{\partial F_{L_2}}{\partial v_2} v_2 - \frac{1}{m}\left(\frac{\partial F_{L_1}}{\partial v_3} + \frac{\partial F_{L_2}}{\partial v_3}\right) v_3 = 0 \\
&-\ddot{v}_1 + \ddot{v}_2 - \frac{E}{I}\dot{v}_1 + \frac{E}{I}\dot{v}_2 + \left(\frac{2ab}{I}\frac{\partial F_{G_1}}{\partial v_1} + \frac{2b^2}{I}\frac{\partial F_{L_1}}{\partial v_1}\right) v_1 \\
&\qquad + \left(\frac{2ab}{I}\frac{\partial F_{G_2}}{\partial v_2} - \frac{2b^2}{I}\frac{\partial F_{L_2}}{\partial v_2}\right) v_2 \\
&\qquad + \left[\frac{2ab}{I}\left(\frac{\partial F_{G_1}}{\partial v_3} + \frac{\partial F_{G_2}}{\partial v_3}\right) + \frac{2b^2}{I}\left(\frac{\partial F_{L_1}}{\partial v_3} - \frac{\partial F_{L_2}}{\partial v_3}\right)\right] v_3 = 0 \\
&\ddot{v}_3 + \frac{D}{m}\dot{v}_3 - \frac{1}{m}\frac{\partial F_{G_1}}{\partial v_1} v_1 - \frac{1}{m}\frac{\partial F_{G_2}}{\partial v_2} v_2 - \frac{1}{m}\left(\frac{\partial F_{G_1}}{\partial v_3} + \frac{\partial F_{G_2}}{\partial v_3}\right) v_3 = 0.
\end{aligned} \tag{22}$$

With magnetic forces and stiffnesses measured by the experiments, the eigenvalues and eigenvectors of a maglev vehicle on a double L-shaped guideway

were calculated with the theoretical model developed in this section. Some very interesting results were obtained from those calculations.

Figure 3 shows that eigenvalues of vehicle motion versus levitation height vary when guidance gaps are fixed ($g_1 = g_2 = 12.7$ mm). The first mode ω_1 shows an uncoupled heave motion; the imaginary part of its eigenvalue is zero. The second and third modes are coupled roll-slip motions. Within a range of height h of 19.0 to 35 mm, the imaginary parts of eigenvalues appear not to be zero. This indicates that within this range flutter does exist for these coupled roll-slip vibrations.

Figure 4 shows eigenvalues of vehicle motion versus lateral location of vehicle when $g_1 = g_2 = g_0 = 25$ mm, and levitation height $h = 7$ mm, respectively. We notice that for the third mode, which presents the transversal motion of vehicle, the real part is zero and the imaginary part is not zero within a certain region. This indicates that the divergence is subjected to the lateral motion of vehicle with those vehicle and guideway parameters. Figure 5 shows the real part of third mode versus lateral location of the vehicle when parameter-equilibrium guidance gap varies as $g_1 = g_2 = g_0 = 10$ m, 15 mm, 20 mm, and 25 mm. We found that the divergence only appears with the case of $g_0 = 25$ mm.

The flutter (Fig. 3) and divergence (Figs. 4 and 5) instabilities have been verified by numerical simulations with a computer code, which has been developed by the authors at Argonne and able to simulate the nonlinear dynamic response of maglev systems with six DOF when the user inputs vehicle and guideway configurations (Cai and Chen, 1995). Figs. 6 and 7 show the time histories of vehicle motions with the vehicle configuration shown in Fig. 2. In

Fig. 6, the slip and roll motions are apparently stable with h_0 = 10 mm, but unstable with h_0 = 10 mm, which indicates that coupled roll-slip flutter indeed occurs. In Fig. 7, divergence of slip and roll motions occurs when g_0 = 25 mm. This is not only indicates that the divergence is subjected to lateral vehicle motion but also reflects the coupling effects between two motions.

Furthermore, the flutter and divergence instabilities were observed from maglev dynamic stability investigation (Cai et al., 1995). It presented a good agreement with the analytical and numerical solutions shown in Figs. 3 to 7, respectively.

CONCLUSIONS

Motion-dependent magnetic forces are the key elements in modeling and understanding the dynamic instabilities of maglev systems. At this time, it appears that very limited data are available for motion-dependent magnetic forces.

Various options can be used to stabilize a maglev system: passive electrodynamic primary suspension damping, active electrodynamic primary suspension damping, passive mechanical secondary suspension, and active mechanical secondary suspension. With a better understanding of vehicle stability characteristics, a better control law can be adopted to ensure a high level of ride comfort and safety.

Computer programs are needed for screening new system concepts, evaluating various designs, and predicting of vehicle response. It appears that the stability characteristics of maglev vehicles under different conditions have not

been studied in detail in existing computer codes. When information on motion-dependent magnetic forces becomes available, the existing computer codes can be significantly improved.

Instabilities of maglev system models have been observed at Argonne National Laboratory and other organizations. An integrated experimental/analytical study of stability characteristics is an important part of any research activities concerning maglev systems.

ACKNOWLEDGMENTS

This work was performed under the sponsorship of the U.S. Army Corps of Engineers and the Federal Railroad Administration, through interagency agreements with the U.S. Department of Energy.

REFERENCES

Cai, Y., and Chen, S. S., (1995), *Numerical Analysis for Dynamic Instability of Electrodynamic Maglev Systems*, The Shock and Vibration Journal, Vol. 2, No. 4, pp. 339-349.

Cai, Y., Chen, S. S., Mulcahy, T. M., and Rote, D. M., (1992), *Dynamic Stability of Maglev Systems*, Proceedings of the 63rd Shock and Vibration Symposium, Las Cruces, NM, October 27-29, 1992, pp. 533-543.

Cai, Y. and Chen, S. S., (1993), *Instability of Electrodynamic Maglev Systems*, Proceedings of the 64th Shock and Vibration Symposium, Ft. Walton Beach, FL, October 25-28, 1993, pp. 319-326.

Cai, Y., Rote, D. M., Chen, S. S., Mulcahy, T. M., Wang, Z. and Zhu, S., Argonne National Laboratory, unpublished information, 1995.

Chen, S. S.,(1987), *Flow-Induced Vibration of Circular Cylindrical Tubes*, Hemisphere Publishing Co., New York.

Chen, S. S., Rote, D. M., and Coffey, H. T., (1992), *A Review of Vehicle/Guideway Interactions in Maglev Systems*, Fluid-Structure Interaction, Transient Thermal-Hydraulics, and Structural Mechanics, ASME, New York, Vol. 231, pp. 81-95.

Chen, S. S., Zhu, S., and Cai, Y., (1993), *On the Unsteady-Motion Theory of Magnetic Forces for Maglev*, Report ANL-93/39, Argonne National Laboratory, Argonne, IL.

Chu, D., and Moon, F. C., (1983), *Dynamic Instabilities in Magnetically Levitated Models*, J. Appl. Phys. **54**(3), pp. 1619-1625.

Davis, L. C., and Wilkie, D. F., (1971), *Analysis of Motion of Magnetic Levitation Systems: Implications,* J. Appl. Phys. **42**(12), pp. 4779-4793.

Moon, F. C., (1974), *Laboratory Studies of Magnetic Levitation in the Thin Track Limit,* IEEE Trans. on Magnetics **MAG-10**(3), pp. 439-442.

Moon, F. C., (1974), *Laboratory Studies of Magnetic Levitation in the Thin Track Limit,* IEEE Trans. on Magnetics **MAG-10**(3), pp. 439-442.

Moon, F. C., (1977), *Vibration Problems in Magnetic Levitation and Propulsion,* Transport Without Wheels, E. R. Laithwaite, ed., Elek Science, London, pp. 122-161.

Ohno, E., Iwamoto, M., and Yamada, T., (1973), *Characteristic of Superconductive Magnetic Suspension and Propulsion for High-Speed Trains,* Proc. IEEE **61**(5), pp. 579-586.

Yabuno, H., Takabayashi, Y., Yoshizawa, M., and Tsujioka, Y., (1989), *Bounding and Pitching Oscillations of a Magnetically Levitated Vehicle Caused by Guideway Roughness*, Int. Conference Maglev 89, pp. 405-410.

Figure Captions

Fig. 1. Displacement components of a maglev system

Fig. 2. Maglev system with a vehicle on a double L-shaped aluminum sheet guideway

Fig. 3. Eigenvalues of maglev system vs. vehicle levitation height with $Y^* =$ 12.7 mm

Fig. 4. Eigenvalues of maglev system vs. lateral location of vehicle with h = 7 mm and $g_0 = 25$ mm

Fig. 5. Real part of eigenvalues of maglev system vs. lateral location of vehicle with h = 7 mm and $g_0 = 10$, 15, 20, and 25 mm

Fig. 6. Time histories of vehicle motions with various vertical air gaps h_0 when $g_0 = 12.7$ mm

Fig. 7. Time histories of vehicle motions with various lateral air gaps g_0 when $h_0 = 7$ mm

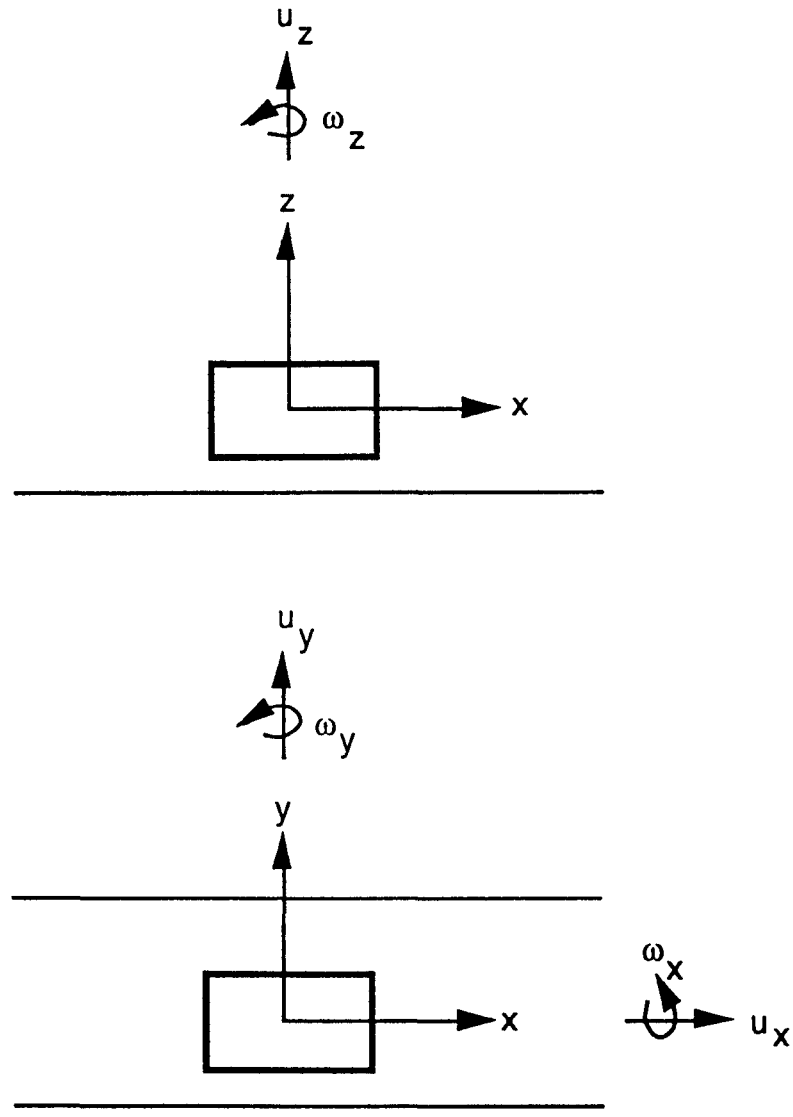

Fig. 1. Displacement components of a maglev system

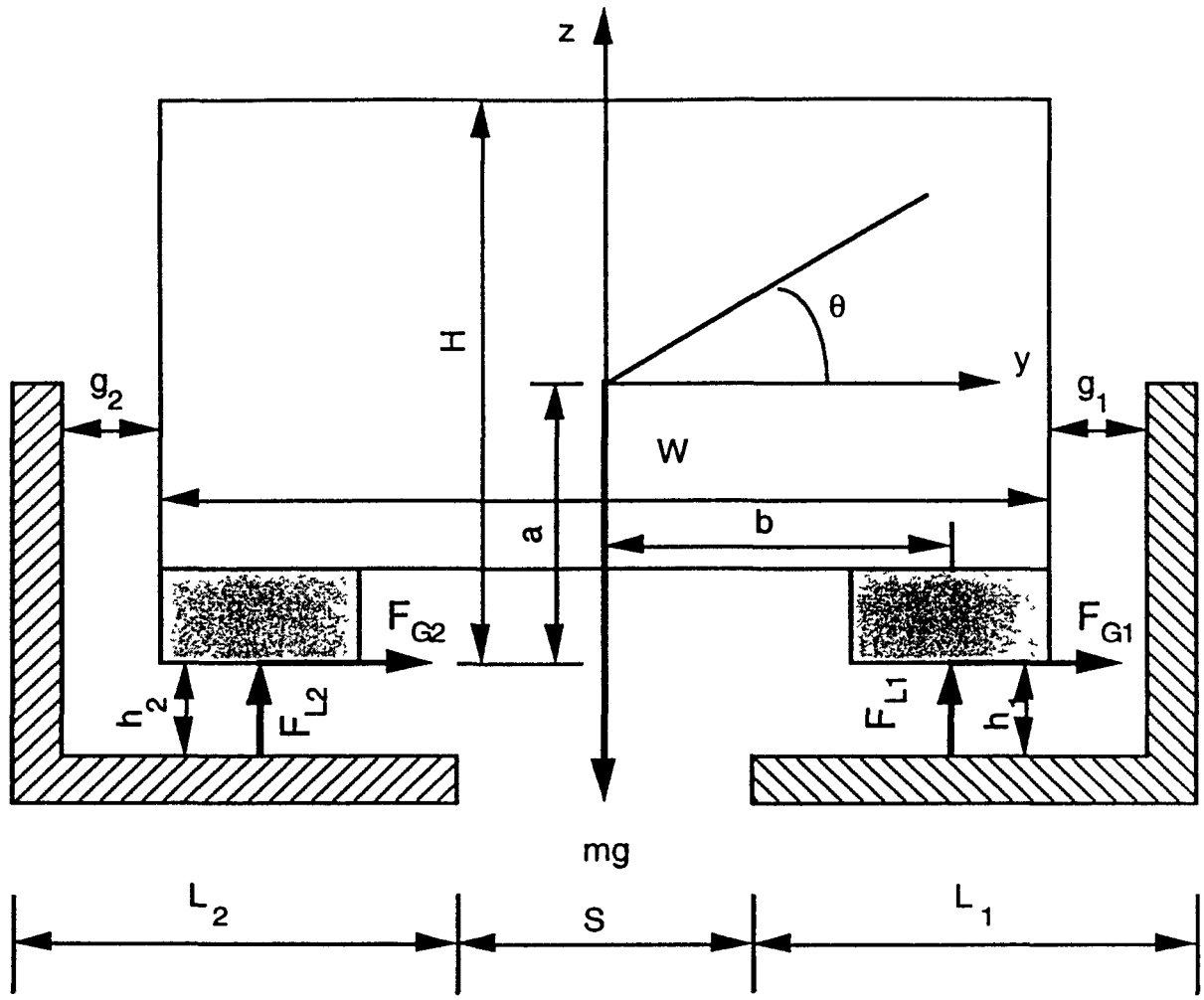

Fig. 2. Maglev system with a vehicle on a double L-shaped aluminum sheet guideway

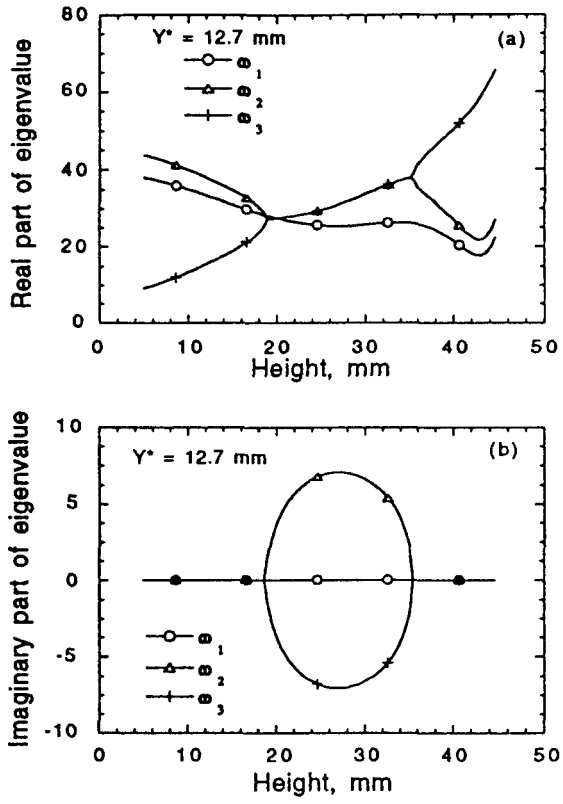

Fig. 3. Eigenvalues of maglev system vs. vehicle levitation height with Y* = 12.7 mm

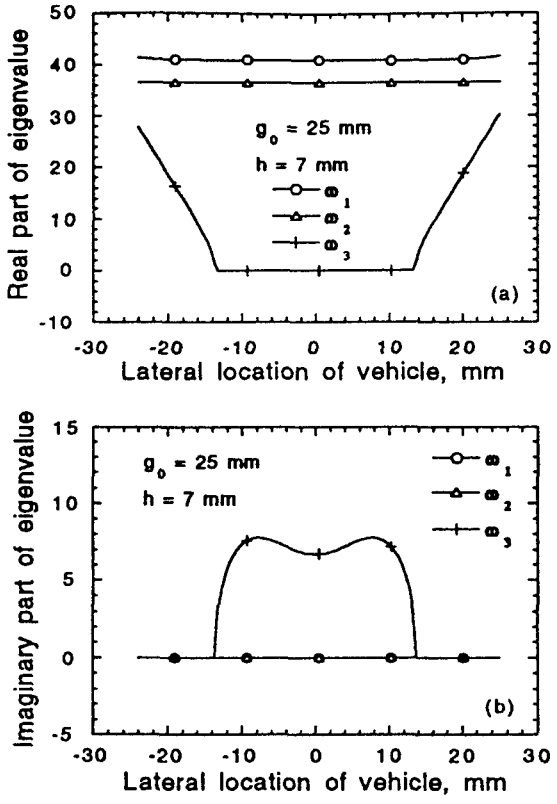

Fig. 4. Eigenvalues of maglev system vs. lateral location of vehicle with h = 7 mm and g_0 = 25 mm

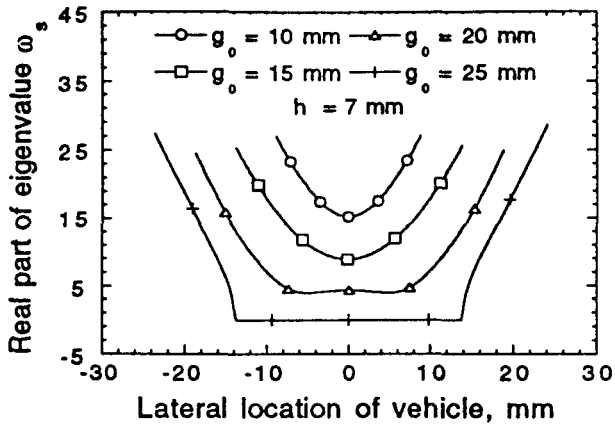

Fig. 5. Real part of eigenvalues of maglev system vs. lateral location of vehicle with h = 7 mm and g_0 = 10, 15, 20, and 25 mm

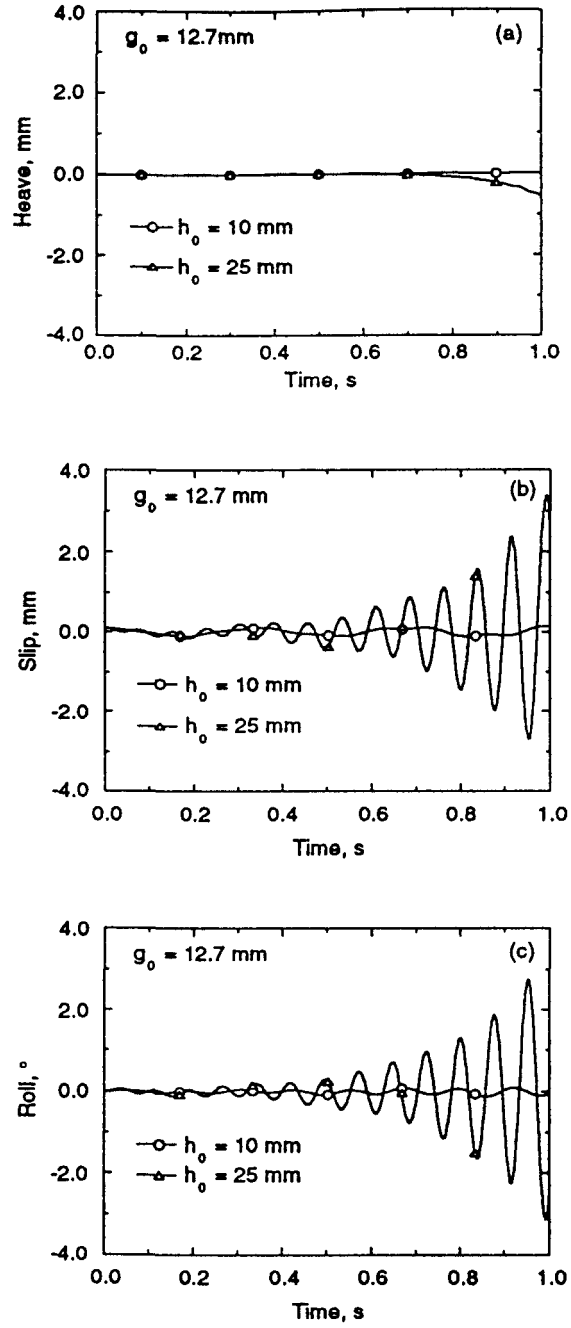

Fig. 6. Time histories of vehicle motions with various vertical air gaps h_0 when g_0 = 12.7 mm.

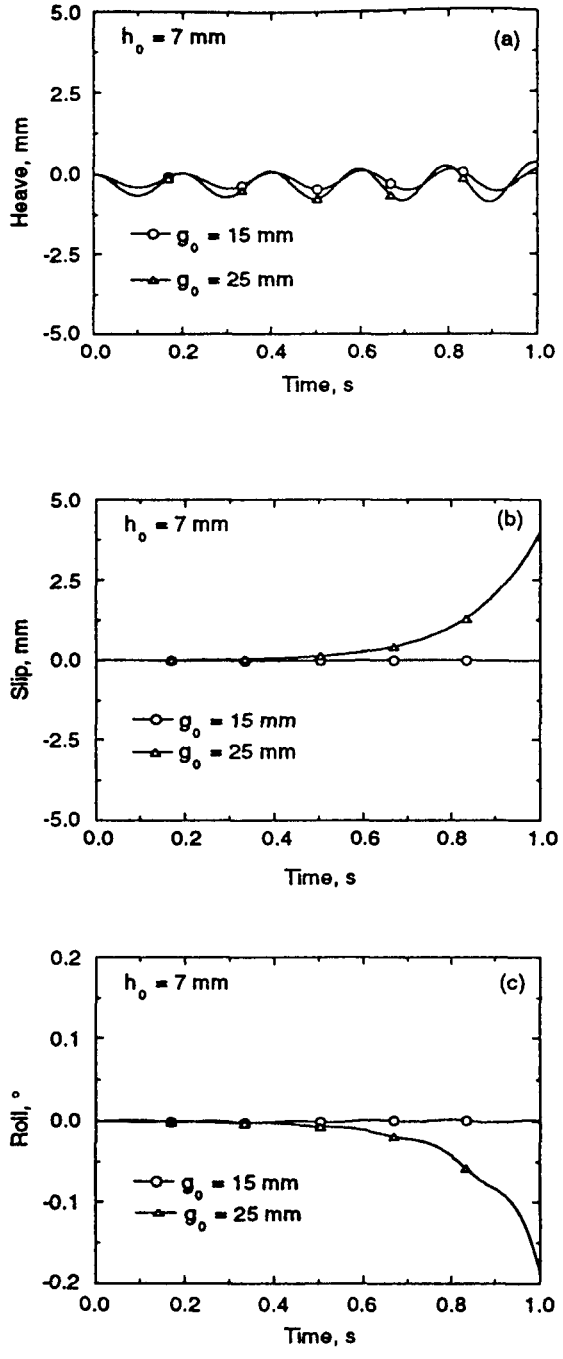

Fig. 7. Time histories of vehicle motions with various lateral air gaps g_0 when $h_0 = 7$ mm.